Editors' Suggestion

Bidirectional Multiphoton Communication between Remote Superconducting Nodes

Joel Grebel,[1] Haoxiong Yan,[1] Ming-Han Chou,[1,2] Gustav Andersson,[1] Christopher R. Conner,[1] Yash J. Joshi,[1] Jacob M. Miller,[1,2] Rhys G. Povey,[1,2] Hong Qiao,[1] Xuntao Wu,[1] and Andrew N. Cleland[1,3,*]

[1]*Pritzker School of Molecular Engineering, University of Chicago, Chicago, Illinois 60637, USA*
[2]*Department of Physics, University of Chicago, Chicago, Illinois 60637, USA*
[3]*Center for Molecular Engineering, Argonne National Laboratory, Lemont, Illinois 60439, USA*

(Received 23 August 2023; accepted 11 December 2023; published 25 January 2024)

Quantum communication test beds provide a useful resource for experimentally investigating a variety of communication protocols. Here we demonstrate a superconducting circuit test bed with bidirectional multiphoton state transfer capability using time-domain shaped wave packets. The system we use to achieve this comprises two remote nodes, each including a tunable superconducting transmon qubit and a tunable microwave-frequency resonator, linked by a 2 m–long superconducting coplanar waveguide, which serves as a transmission line. We transfer both individual and superposition Fock states between the two remote nodes, and additionally show that this bidirectional state transfer can be done simultaneously, as well as being used to entangle elements in the two nodes.

DOI: 10.1103/PhysRevLett.132.047001

Long-range, high-fidelity communication of quantum information has applications in several areas [1], including secure communication using quantum key cryptography [2], as well as serving as the backbone for a future quantum Internet [3]. These applications require sources of entangled photons, preferably on-demand, to perform most quantum cryptographic functions. Photons at optical frequencies are a natural choice for the communication medium, due to their high energies compared to ambient thermal energies, their low propagation loss at room temperature, and widely available fiber communication technology. However, high-fidelity and high-rate sources of on-demand entangled photons are still lacking at optical frequencies, yielding to date low information transfer rates [4–8]. At microwave frequencies, superconducting circuits provide a flexible platform for designing high-fidelity control of computational elements with reasonably low-loss memory elements, and can deterministically generate microwave photons entangled with qubits. Combined with variable superconducting couplers, these elements can be used to experimentally test long-range communication protocols [9] with itinerant photon wave packets [10–19], as well as modular quantum computing approaches, using the standing modes in a weakly coupled communication waveguide [20–23]. Several experiments using superconducting circuits have demonstrated deterministic transfer of both single [14–16] and multiphoton states [17] between remote nodes, using time-symmetric shaped wave packets to improve transfer fidelity [24]. However, with the exception of Refs. [16,19], these all involved the use of lossy microwave circulators, thus only supporting communication in one direction.

Here we demonstrate bidirectional, multiphoton state transfer with shaped wave packets between two remote superconducting qubit nodes, eliminating the microwave circulators used in earlier experiments [14,15,17]. Circulators are useful for preventing unwanted reflections from emitted signals, simplifying the tune-up and operation of these circuits. However, existing broadband commercial circulators cannot reverse their polarity *in situ*, and further are a significant source of loss; while broadband parametric circulators may overcome these limitations [25,26], they are not yet available. Here, we implement itinerant bidirectional communication, where itinerant means the pulsed signals have time-domain envelopes shorter than the length of the transmission line; we achieve this by using fast dynamic couplers at each node, allowing us to complete signal transfers with low reflection rates and sufficient speed that interference between emission and reflection signals can be avoided [16].

The experimental device is shown in Fig. 1. Each of the two nodes comprises a frequency-tunable superconducting Xmon qubit [27] $Q1$ ($Q2$), capacitively coupled to a frequency-tunable resonator $R1$ ($R2$), which is in turn connected via a variable coupler [28] to one end of a 2 m–long, 50 Ω coplanar waveguide. The tunable resonators are implemented as a resonant section of coplanar waveguide terminated by a superconducting quantum interference device (SQUID) [29], connected to ground through the variable coupler. Control flux lines allow tuning the resonator over a range of 1.5 GHz, limited in the experiment to 0.5 GHz by the control electronics. The variable couplers afford control of the coupling strength of the resonator to the 2 m–long transmission line, where the resonator decay rate $\kappa_r/2\pi$ into the transmission line can be

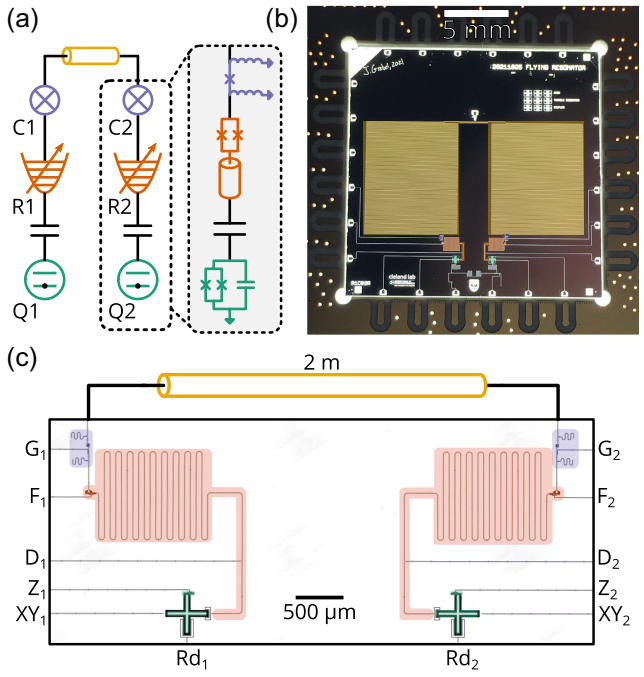

FIG. 1. Experimental layout. (a) Block diagram for the experiment, comprising two tunable qubits $Q1$, $Q2$ (green), capacitively coupled to two tunable resonators $R1$, $R2$ (orange), in turn coupled via two variable couplers $C1$, $C2$ (purple) to a 2 m–long waveguide (yellow). Circuit representations of these elements are shown in the dashed box. (b) Backside-illuminated optical photograph of fabricated device with false coloring, showing all components including the 2 m–long coplanar waveguide, as well as the printed circuit board to which the die is wirebonded for signal routing. A test pad for detecting shorts is directly above the midpoint of the waveguide. The test pad is physically disconnected prior to the experiment, removing the electrical connection to the waveguide. Test pads and trial Josephson junctions for measuring junction resistances are located to the top right of the waveguide. (c) Optical micrograph of device with false coloring corresponding to components shown in panel (a). The coplanar waveguide is patterned on the same die but is cropped from this image; see panel (b). Microwave XY lines are used to excite the qubits (i.e., for X and Y rotations), Z lines control the qubit frequency (yielding a Z rotation referenced to a system clock), D lines displace the resonators for Wigner tomography, F lines control the resonator frequency, G lines control the coupler, and Rd refers to the readout resonators. Subscripts indicate nodes 1 or 2.

varied dynamically from 0 to 55 MHz, with control signals as short as 3 ns, limited by control-line filtering. The transmission line itself is a 50 Ω coplanar waveguide, galvanically connected to each variable coupler. All components are fabricated on a single 2 cm × 2 cm sapphire die, shown in a back-lit optical photograph in Fig. 1(b). Fabrication details are provided in Ref. [30]. The device was wire-bonded to a copper printed circuit board that was in turn placed in an aluminum enclosure, the latter placed in a double magnetic shield mounted to the 10 mK mixing chamber of a dilution refrigerator. A wiring diagram showing the cabling for the dilution refrigerator and a schematic for the control and readout circuitry are shown in the Supplemental Material [30].

A standard characterization of the qubits yields characteristic lifetimes $T_{1,Q1} = 20$ μs and $T_{1,Q2} = 22$ μs at the qubit operating frequencies of $f_{Q1} = 4.57$ GHz and $f_{Q2} = 4.5$ GHz. The qubit Ramsey coherence times T_2 at the same operating frequencies are 2.6 μs and 0.56 μs, respectively.

To characterize the tunable resonators, we swap single excitations from the qubits to their respective resonators by tuning the excited qubit into resonance with the resonator for a calibrated time, with the variable couplers turned off. Using the qubits to monitor the subsequent resonator decay, we measure characteristic T_1 and T_2 times of $T_{1,R1} = 4.57$ μs, $T_{1,R2} = 0.86$ μs, $T_{2,R1} = 0.95$ μs, and $T_{2,R2} = 0.9$ μs. All qubit-resonator swaps are measured at frequency $f_R = 4.058$ GHz with qubit-resonator coupling strength $g_{\mathrm{QR}}/2\pi = 6.8$ MHz set by the geometric capacitance $C = 1.4$ fF connecting these elements.

We characterize the transmission waveguide by swapping excitations into individual standing waveguide modes as shown in Fig. 2(a), at weak coupling $g_{RW} \ll \omega_{FSR}$, with $g_{RW}/2\pi < 3.4$ MHz as the coupling strength between the resonator and waveguide, and $\omega_{FSR}/2\pi = 31$ MHz the waveguide free spectral range. The waveguide T_1 coherence times are in the range of 4–5 μs. At stronger coupling, we emit itinerant wave packets into the waveguide, which requires coupling to a number of adjacent waveguide modes. Figure 2(b) shows a Ramsey-like experiment with $\pi/2$ pulses on $Q2$ at the beginning and end of the pulse sequence, where we emit and then recapture a superposition $|0\rangle + |1\rangle$ state in $R2$ for different resonator frequencies. The return time for the pulses is independent of the resonator frequency in this regime; fringes at different frequencies indicate phase coherence in the waveguide. See Ref. [30] for more characterization details.

We prepare Fock states in each tunable resonator by exciting the adjacent qubit, then resonantly swapping photons one at a time into the resonator [55]. In Figs. 3(a) and 3(b), we swap an $n = 1$ Fock state between the resonators via the communication waveguide, by first exciting either resonator via its adjacent qubit with both resonators tuned to f_R and controlling the variable couplers with calibrated pulses to perform an itinerant release-and-catch transfer of the excitation [16]. We then swap the receiving resonator's excitation to the corresponding qubit for measurement. We release and subsequently capture the wave packet by dynamically tuning the coupling strength for each coupler, and we optimize the state transfer using Bayesian optimization [56]. During this process, we hold each resonator's frequency constant by applying a stabilizing flux pulse to its SQUID; this corrects for frequency changes due to the changing loading electrical circuit, as well as flux

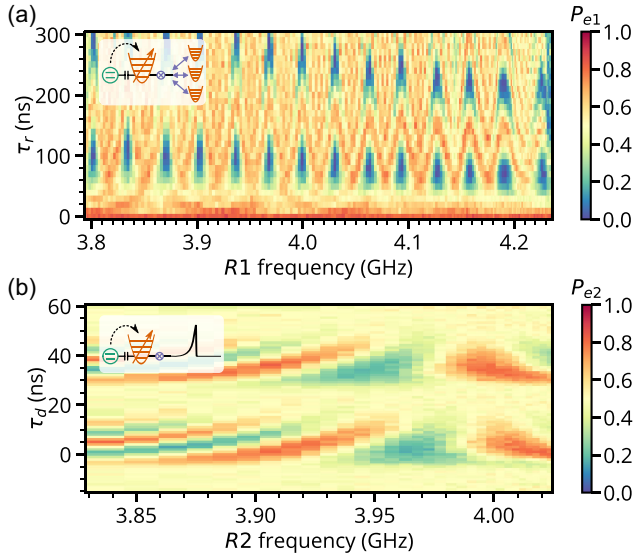

FIG. 2. (a) Standing waveguide modes seen by $R1$ at weak coupling. After a single excitation is swapped into $R1$, the coupling to the waveguide is turned on for time τ_r, while the resonator is held at a constant frequency. (b) Ramsey-like experiment showing itinerant emission and recapture of a $|0\rangle + |1\rangle$ state in $R2$. The superposition state is swapped from $Q2$ to $R2$, emitted and recaptured from $R2$ with 20 ns rectangular pulses separated by delay τ_d, while the resonator is held at a constant frequency, swapped back to $Q2$, and a $\pi/2$ pulse is applied to $Q2$ before measurement. P_{e1} and P_{e2} are the excitation probabilities of qubits $Q1$ and $Q2$, respectively, after the experimental pulse sequences. Detailed pulse sequences are given in Ref. [30].

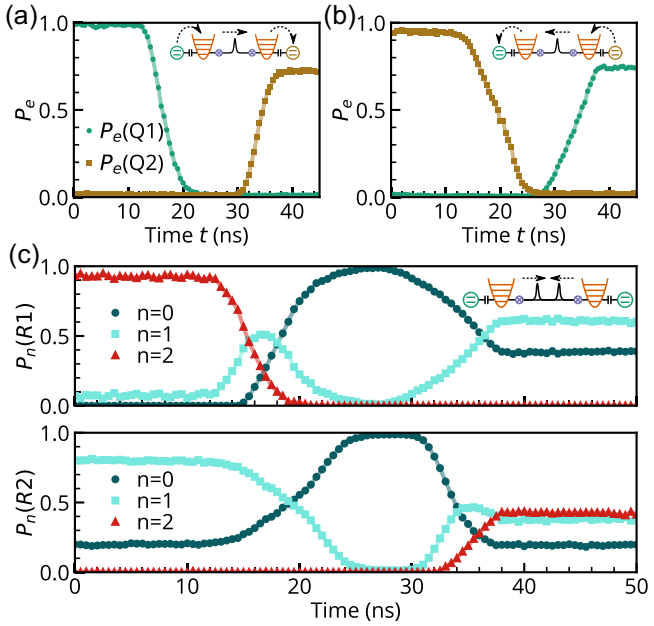

FIG. 3. Transfer of excited qubit states, from (a) qubit $Q1$ to qubit $Q2$ and from (b) $Q2$ to $Q1$. We excite the emitting qubit, swap the excitation to the adjacent resonator, transmit the excitation as a wave packet to the distant resonator by time-varying control of the couplers between the resonators and waveguide, then finally swap to the receiving qubit. Lines are a guide for the eye. (c) Simultaneous state swaps between the resonators. We initialize resonator $R1$ in a two-photon Fock state while initializing resonator $R2$ in a one-photon Fock state. These states are simultaneously released into the transmission line as itinerant wave packets that are then captured by the receiving resonators, and we use the associated qubit to analyze its associated resonator's final state. The population of each resonator's Fock states $|F_n\rangle$, $n = 0, 1, 2$ is shown as a function of time. Detailed pulse sequences are given in Ref. [30].

cross-talk. We transfer single photons in either direction, with an efficiency of 0.72 for $Q1 \rightarrow Q2$ transfers, and an efficiency of 0.74 for the reverse direction. Here, efficiency is defined as $\mathcal{E} = \langle P_j \rangle / \langle P_i \rangle$, where $P_{i,j}$ are the release and capture qubit populations, respectively. The inefficiency is likely dominated by nonideal pulse shaping and timing, as the inverse loss rate in the system is well characterized and significantly longer than the transfer time.

To demonstrate bidirectional itinerant state transfer, we prepare dual resonator states using the adjacent qubits and then simultaneously release these into the communication waveguide, using the qubits to monitor the resonator populations. In Fig. 3(c), we show the schematic process, where we prepare resonator $R1$ with a two-photon Fock state while preparing resonator $R2$ with a one-photon Fock state. We then use both variable couplers to perform a simultaneous itinerant release-and-catch of photons transmitted in each direction in the communication waveguide. To reconstruct the resulting population in the resonators, we resonantly interact the resonator with its corresponding qubit for a variable length of time, monitoring the qubit excited state probability. We then fit the time-dependent response to a model Hamiltonian for the combined system [57]. The reconstructed resonator Fock state probabilities for Fock states $n = 0, 1, 2$ are shown in Fig. 3 as a function of time. Due to the use of slightly different control pulses, in this experiment the resonator one-photon transfer efficiency is 0.82, while the two-photon transfer efficiency is 0.64. The infidelity of the initial $|1\rangle$ state in $R2$ is primarily due to the short resonator lifetime (< 1 μs), combined with the long state preparation sequence. Further details about pulse sequences are given in Ref. [30].

We can also use this system to generate and transfer more complex quantum states. In Fig. 4(a), we show the preparation and transfer of superposition Fock states. We prepare the $|0\rangle + |1\rangle$ superposition states in resonator $R1$ by swapping a $|g\rangle + |e\rangle$ state from qubit $Q1$, achieving a state fidelity $\mathcal{F} = 0.99(6)$. We perform an itinerant state transfer via the communication channel to resonator $R2$ with fidelity $\mathcal{F} = 0.94(0)$, where $\mathcal{F}(\rho, \sigma) = \mathrm{tr}\sqrt{\rho^{1/2}\sigma\rho^{1/2}}$ of the measured density matrix ρ to the ideal state σ. In a similar fashion, we prepare the $|0\rangle + |2\rangle$ superposition in $R2$ by exciting $Q1$ to the $|g\rangle + |f\rangle$ state with two subsequent swaps to $R1$, achieving a fidelity $\mathcal{F} = 0.95(2)$. The $|0\rangle + |2\rangle$ superposition is then transferred by wave packet

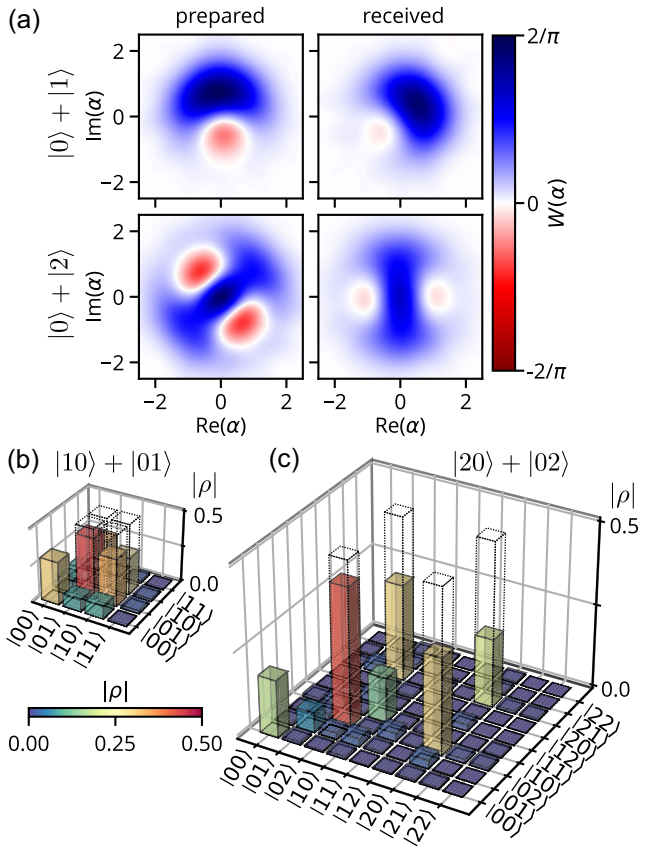

FIG. 4. (a) Transfer of superposition Fock states. We prepare $|0\rangle + |1\rangle$ and $|0\rangle + |2\rangle$ states in resonator $R1$ and transfer these as itinerant wave packets to resonator $R2$. We use the corresponding qubits to reconstruct the Wigner tomograms in both resonators, as described in the main text. The lower graphs show NOON states $|n0\rangle + |0n\rangle$ with (b) $n = 1$ and (c) $n = 2$ itinerant transfers between the two tunable resonators. State preparation is described in the main text. Dotted lines indicate the ideal NOON states, while transparent colored bars are the reconstructed density matrices.

via the communication channel to $R2$, with fidelity $\mathcal{F} = 0.82(3)$. The Wigner tomograms in the figure are reconstructed by using convex optimization to find the most likely state that fits the Fock distribution as a function of displacement [58,59]. To measure the final resonator Fock state distribution, we tune the qubit, initially in its ground state, to the resonator frequency, and fit the subsequent qubit oscillations to a model system [30,57]. The phase difference between the prepared and received states is possibly due to the resonator frequency varying slightly during wave packet release and capture, due to nonideal control pulses. Wigner tomograms of the raw parity data are given in [30].

To demonstrate the generation of remote entanglement in this system, shown in Fig. 4(b), we create NOON states, superposition states in which N-photon states in one resonator are superposed with vacuum states in the other resonator, in the form $|\psi\rangle = (1/\sqrt{2})(|N0\rangle - |0N\rangle)$. In Fig. 4(b), for the $N = 1$ NOON state, we prepare a one-photon Fock state in $R1$, and then, via an itinerant transfer, move half the population to $R2$. We then measure the joint resonator state with bipartite Wigner tomography [60], using convex optimization to find the most likely state given by the joint resonator Fock distribution as a function of displaced resonator states [58,59]. Similarly to the single resonator case, we measure the joint resonator Fock distribution by tuning both qubits, initially in their ground states, into resonance with their respective resonators, and then we fit the resulting qubit population oscillations to a model system [30,60]. The fidelity of the prepared state is found to be $\mathcal{F} = 0.82(7)$. In Fig. 4(c), for the $N = 2$ NOON state, we first prepare a one-excitation Bell state $(|eg\rangle - |ge\rangle)/\sqrt{2}$ in the two qubits, by swapping half an excitation from $Q1$ to $R1$, followed by an itinerant transfer from $R1$ to $R2$, and finally swapping the half-excitation to $Q2$. We next excite the $e - f$ transition in each qubit, resulting in the state $(|fg\rangle - |gf\rangle)/\sqrt{2}$, and then transfer the qubit populations to the resonators with two subsequent swaps, resulting in the final resonator state $(|20\rangle - |02\rangle)/\sqrt{2}$. The fidelity to the ideal state is $\mathcal{F} = 0.78(0)$. Figures 4(b) and 4(c) show the reconstructed absolute value of the density matrices for the two states. The major sources of infidelity are photon loss during the transfer process and while stored in the resonators.

In conclusion, we demonstrate multiphoton bidirectional communication between two quantum-coherent superconducting nodes coupled by a 2 m–long coplanar waveguide, with states sent using itinerant photons whose pulse lengths of 0.45 m are significantly less than the 2 m length of the waveguide. Future experiments might transfer multiphoton qubits such as the cat [61] or GKP [62] encoding states between resonators in the testbed. Other communication protocols might be achieved by dynamically varying both the resonator frequencies and the coupling strength of each resonator to the waveguide during wave packet emission and capture. We can judge the relative performance of different communication protocols using a single system—e.g., using final-state fidelities. Tens of individual waveguide modes can be addressed by each node; this system thus has further potential as a quantum random access memory [63]. Additional nodes may be connected to the network by adding multiple coupled waveguides to each resonator, with nodes in separate modules if needed [22]. The most significant limitations in this system are the challenges in the time-domain control of both the couplers and resonators, which has to account for circuit loading, flux cross-talk, and cable-related pulse distortions. Higher fidelities might be achieved using machine learning techniques such as those implemented in Refs. [64,65]; more precise pulse control with faster electronics and fewer control wiring filters; and a longer waveguide that allows longer-duration itinerant photon pulse shapes, making time-domain control less challenging. Additional considerations for multiphoton transfer

state transfer between separate chips are discussed in the Supplemental Material [30].

Correspondence and requests for materials should be addressed to A. N. Cleland.

We thank P. J. Duda for helpful discussions and W. D. Oliver and G. Calusine at Lincoln Laboratories for the provision of a traveling-wave parametric amplifier. Financial support was provided by the NSF QLCI for HQAN (NSF Grant No. 2016136), the U.S. Department of Energy Office of Science National Quantum Information Science Research Centers, the Army Research Office-Laboratory for Physical Sciences (Contract No. W911NF-23-1-0077), and the University of Chicago MRSEC (NSF Grant No. DMR-2011854). We made use of the Pritzker Nanofabrication Facility, partially supported by SHyNE, a node of the National Science Foundation's National Nanotechnology Coordinated Infrastructure (NSF Grant No. NNCI ECCS-2025633). A. N. C. was supported in part by the DOE, Office of Basic Energy Sciences.

J. G. designed and fabricated the devices, performed the experiment, and analyzed the data. H. Y., M. H. C., and G. A. provided suggestions for measurement and data analysis. A. N. C. advised on all efforts. All authors contributed to discussion and production of the manuscript.

The authors declare no competing financial interests.

*Corresponding author: anc@uchicago.edu

[1] N. Gisin and R. Thew, Quantum communication, Nat. Photonics **1**, 165 (2007).
[2] A. K. Ekert, Quantum cryptography based on Bell's theorem, Phys. Rev. Lett. **67**, 661 (1991).
[3] H. J. Kimble, The quantum internet, Nature (London) **453**, 1023 (2008).
[4] A. Reiserer, Colloquium: Cavity-enhanced quantum network nodes, Rev. Mod. Phys. **94**, 041003 (2022).
[5] H.-J. Briegel, W. Dür, J. I. Cirac, and P. Zoller, Quantum repeaters: The role of imperfect local operations in quantum communication, Phys. Rev. Lett. **81**, 5932 (1998).
[6] W. J. Munro, K. Azuma, K. Tamaki, and K. Nemoto, Inside quantum repeaters, IEEE J. Sel. Top. Quantum Electron. **21**, 78 (2015).
[7] J. Yin *et al.*, Satellite-based entanglement distribution over 1200 kilometers, Science **356**, 1140 (2017).
[8] D. Du, P. Stankus, O.-P. Saira, M. Flament, S. Sagona-Stophel, M. Namazi, D. Katramatos, and E. Figueroa, An elementary 158 km long quantum network connecting room temperature quantum memories, arXiv:2101.12742.
[9] M. Casariego *et al.*, Propagating quantum microwaves: Towards applications in communication and sensing, Quantum Sci. Technol. **8**, 023001 (2023).
[10] Y. Yin, Y. Chen, D. Sank, P. J. J. O'Malley, T. C. White, R. Barends, J. Kelly, E. Lucero, M. Mariantoni, A. Megrant, C. Neill, A. Vainsencher, J. Wenner, A. N. Korotkov, A. N. Cleland, and J. M. Martinis, Catch and release of microwave photon states, Phys. Rev. Lett. **110**, 107001 (2013).
[11] J. Wenner, Y. Yin, Y. Chen, R. Barends, B. Chiaro, E. Jeffrey, J. Kelly, A. Megrant, J. Y. Mutus, C. Neill, P. J. J. O'Malley, P. Roushan, D. Sank, A. Vainsencher, T. C. White, A. N. Korotkov, A. N. Cleland, and J. M. Martinis, Catching time-reversed microwave coherent state photons with 99.4% absorption efficiency, Phys. Rev. Lett. **112**, 210501 (2014).
[12] M. Pierre, I.-M. Svensson, S. Raman Sathyamoorthy, G. Johansson, and P. Delsing, Storage and on-demand release of microwaves using superconducting resonators with tunable coupling, Appl. Phys. Lett. **104**, 232604 (2014).
[13] S. J. Srinivasan, N. M. Sundaresan, D. Sadri, Y. Liu, J. M. Gambetta, T. Yu, S. M. Girvin, and A. A. Houck, Time-reversal symmetrization of spontaneous emission for quantum state transfer, Phys. Rev. A **89**, 033857 (2014).
[14] P. Kurpiers, P. Magnard, T. Walter, B. Royer, M. Pechal, J. Heinsoo, Y. Salathé, A. Akin, S. Storz, J.-C. Besse, S. Gasparinetti, A. Blais, and A. Wallraff, Deterministic quantum state transfer and remote entanglement using microwave photons, Nature (London) **558**, 264 (2018).
[15] P. Campagne-Ibarcq, E. Zalys-Geller, A. Narla, S. Shankar, P. Reinhold, L. Burkhart, C. Axline, W. Pfaff, L. Frunzio, R. J. Schoelkopf, and M. H. Devoret, Deterministic remote entanglement of superconducting circuits through microwave two-photon transitions, Phys. Rev. Lett. **120**, 200501 (2018).
[16] Y. P. Zhong, H.-S. Chang, K. J. Satzinger, M.-H. Chou, A. Bienfait, C. R. Conner, É. Dumur, J. Grebel, G. A. Peairs, R. G. Povey, D. I. Schuster, and A. N. Cleland, Violating Bell's inequality with remotely connected superconducting qubits, Nat. Phys. **15**, 741 (2019).
[17] C. J. Axline, L. D. Burkhart, W. Pfaff, M. Zhang, K. Chou, P. Campagne-Ibarcq, P. Reinhold, L. Frunzio, S. M. Girvin, L. Jiang, M. H. Devoret, and R. J. Schoelkopf, On-demand quantum state transfer and entanglement between remote microwave cavity memories, Nat. Phys. **14**, 705 (2018).
[18] P. Magnard, S. Storz, P. Kurpiers, J. Schär, F. Marxer, J. Lütolf, T. Walter, J.-C. Besse, M. Gabureac, K. Reuer, A. Akin, B. Royer, A. Blais, and A. Wallraff, Microwave quantum link between superconducting circuits housed in spatially separated cryogenic systems, Phys. Rev. Lett. **125**, 260502 (2020).
[19] J. Qiu, Y. Liu, J. Niu, L. Hu, Y. Wu, L. Zhang, W. Huang, Y. Chen, J. Li, S. Liu *et al.*, Deterministic quantum teleportation between distant superconducting chips, arXiv:2302.08756.
[20] H.-S. Chang, Y. P. Zhong, A. Bienfait, M.-H. Chou, C. R. Conner, E. Dumur, J. Grebel, G. A. Peairs, R. G. Povey, K. J. Satzinger, and A. N. Cleland, Remote entanglement via adiabatic passage using a tunably dissipative quantum communication system, Phys. Rev. Lett. **124**, 240502 (2020).
[21] L. D. Burkhart, J. D. Teoh, Y. Zhang, C. J. Axline, L. Frunzio, M. H. Devoret, L. Jiang, S. M. Girvin, and R. J. Schoelkopf, Error-detected state transfer and entanglement in a superconducting quantum network, PRX Quantum **2**, 030321 (2021).

[22] Y. Zhong, H.-S. Chang, A. Bienfait, t. Dumur, M.-H. Chou, C. R. Conner, J. Grebel, R. G. Povey, H. Yan, D. I. Schuster, and A. N. Cleland, Deterministic multi-qubit entanglement in a quantum network, Nature (London) **590**, 571 (2021).
[23] J. Niu, L. Zhang, Y. Liu, J. Qiu, W. Huang, J. Huang, H. Jia, J. Liu, Z. Tao, W. Wei, Y. Zhou, W. Zou, Y. Chen, X. Deng, X. Deng, C. Hu, L. Hu, J. Li, D. Tan, Y. Xu, F. Yan, T. Yan, S. Liu, Y. Zhong, A. N. Cleland, and D. Yu, Low-loss interconnects for modular superconducting quantum processors, Natl. Electron. Rev. **6**, 235 (2023).
[24] J. I. Cirac, P. Zoller, H. J. Kimble, and H. Mabuchi, Quantum state transfer and entanglement distribution among distant nodes in a quantum network, Phys. Rev. Lett. **78**, 3221 (1997).
[25] M. Beck, M. Selvanayagam, A. Carniol, S. Cairns, and C. Mancini, Wideband Josephson parametric isolator, Phys. Rev. Appl. **20**, 034054 (2023).
[26] R. Kwende, T. White, and O. Naaman, Josephson parametric circulator with same-frequency signal ports, 200 MHz bandwidth, and high dynamic range, Appl. Phys. Lett. **122**, 224001 (2023).
[27] R. Barends, J. Kelly, A. Megrant, D. Sank, E. Jeffrey, Y. Chen, Y. Yin, B. Chiaro, J. Mutus, C. Neill, P. O'Malley, P. Roushan, J. Wenner, T. C. White, A. N. Cleland, and J. M. Martinis, Coherent Josephson qubit suitable for scalable quantum integrated circuits, Phys. Rev. Lett. **111**, 080502 (2013).
[28] Y. Chen *et al.*, Qubit architecture with high coherence and fast tunable coupling, Phys. Rev. Lett. **113**, 220502 (2014).
[29] M. Sandberg, C. M. Wilson, F. Persson, T. Bauch, G. Johansson, V. Shumeiko, T. Duty, and P. Delsing, Tuning the field in a microwave resonator faster than the photon lifetime, Appl. Phys. Lett. **92**, 203501 (2008).
[30] See Supplemental Material at http://link.aps.org/supplemental/10.1103/PhysRevLett.132.047001 for details on experimental setup, numerical analysis, and device tuneup, with Refs. [31–54].
[31] J. S. Kelly, Fault-tolerant superconducting qubits, Ph.D. thesis, University of California, Santa Barbara, 2015.
[32] A. Dunsworth *et al.*, Characterization and reduction of capacitive loss induced by sub-micron Josephson junction fabrication in superconducting qubits, Appl. Phys. Lett. **111**, 022601 (2017).
[33] A. Dunsworth *et al.*, A method for building low loss multi-layer wiring for superconducting microwave devices, Appl. Phys. Lett. **112**, 063502 (2018).
[34] J. Grebel, Bidirectional multi-photon communication between remote superconducting resonators, Ph.D. thesis, The University of Chicago, 2023.
[35] S. Huang, B. Lienhard, G. Calusine, A. Vepsäläinen, J. Braumüller, D. K. Kim, A. J. Melville, B. M. Niedzielski, J. L. Yoder, B. Kannan, T. P. Orlando, S. Gustavsson, and W. D. Oliver, Microwave package design for superconducting quantum processors, PRX Quantum **2**, 020306 (2021).
[36] M. Esposito, A. Ranadive, L. Planat, and N. Roch, Perspective on traveling wave microwave parametric amplifiers, Appl. Phys. Lett. **119**, 120501 (2021).
[37] M. Wallquist, V. S. Shumeiko, and G. Wendin, Selective coupling of superconducting charge qubits mediated by a tunable stripline cavity, Phys. Rev. B **74**, 224506 (2006).
[38] M. R. Geller, E. Donate, Y. Chen, M. T. Fang, N. Leung, C. Neill, P. Roushan, and J. M. Martinis, Tunable coupler for superconducting Xmon qubits: Perturbative nonlinear model, Phys. Rev. A **92**, 012320 (2015).
[39] D. M. Pozar, *Microwave Engineering*, 4th ed. (John Wiley & Sons, New York, 2009).
[40] S. E. Nigg, H. Paik, B. Vlastakis, G. Kirchmair, S. Shankar, L. Frunzio, M. H. Devoret, R. J. Schoelkopf, and S. M. Girvin, Black-box superconducting circuit quantization, Phys. Rev. Lett. **108**, 240502 (2012).
[41] A. H. Kiilerich and K. Mølmer, Input-output theory with quantum pulses, Phys. Rev. Lett. **123**, 123604 (2019).
[42] J. R. Johansson, P. D. Nation, and F. Nori, Qutip: An open-source PYTHON framework for the dynamics of open quantum systems, Comput. Phys. Commun. **183**, 1760 (2012).
[43] A. Bienfait, K. J. Satzinger, Y. P. Zhong, H.-S. Chang, M.-H. Chou, C. R. Conner, É. Dumur, J. Grebel, G. A. Peairs, R. G. Povey, and A. N. Cleland, Phonon-mediated quantum state transfer and remote qubit entanglement, Science **364**, 368 (2019).
[44] D. T. Sank, Fast, accurate state measurement in superconducting qubits, Ph.D. thesis, University of California, Santa Barbara, 2014.
[45] H. Yan, X. Wu, A. Lingenfelter, Y. J. Joshi, G. Andersson, C. R. Conner, M.-H. Chou, J. Grebel, J. M. Miller, R. G. Povey *et al.*, Broadband bandpass Purcell filter for circuit quantum electrodynamics, Appl. Phys. Lett. **123**, 134001 (2023).
[46] Z. L. Wang, Y. P. Zhong, L. J. He, H. Wang, J. M. Martinis, A. N. Cleland, and Q. W. Xie, Quantum state characterization of a fast tunable superconducting resonator, Appl. Phys. Lett. **102**, 163503 (2013).
[47] Y.-X. Liu, L. F. Wei, and F. Nori, Generation of nonclassical photon states using a superconducting qubit in a microcavity, Europhys. Lett. **67**, 941 (2004).
[48] A. Wallraff, D. I. Schuster, A. Blais, J. M. Gambetta, J. Schreier, L. Frunzio, M. H. Devoret, S. M. Girvin, and R. J. Schoelkopf, Sideband transitions and two-tone spectroscopy of a superconducting qubit strongly coupled to an on-chip cavity, Phys. Rev. Lett. **99**, 050501 (2007).
[49] Z. Chen, Metrology of quantum control and measurement in superconducting qubits, Ph.D. thesis, University of California, Santa Barbara, 2018.
[50] C. W. Gardiner and M. J. Collett, Input and output in damped quantum systems: Quantum stochastic differential equations and the master equation, Phys. Rev. A **31**, 3761 (1985).
[51] S. Haroche and J.-M. Raimond, *Exploring the Quantum: Atoms, Cavities, and Photons* (Oxford University Press, New York, 2006).
[52] C. R. Conner, A. Bienfait, H.-S. Chang, M.-H. Chou, E. Dumur, J. Grebel, G. A. Peairs, R. G. Povey, H. Yan, Y. P. Zhong, and A. N. Cleland, Superconducting qubits in a flip-chip architecture, Appl. Phys. Lett. **118**, 232602 (2021).
[53] J. Wenner, M. Neeley, R. C. Bialczak, M. Lenander, E. Lucero, A. D. O'Connell, D. Sank, H. Wang, M. Weides, A. N. Cleland, and J. M. Martinis, Wirebond crosstalk and cavity modes in large chip mounts for superconducting qubits, Supercond. Sci. Technol. **24**, 065001 (2011).

[54] Y. Zhong, Violating Bell's inequality with remotely-connected superconducting qubits, Ph.D. thesis, Pritzker School of Molecular Engineering, University of Chicago, Chicago IL (2019).
[55] M. Hofheinz, E. M. Weig, M. Ansmann, R. C. Bialczak, E. Lucero, M. Neeley, A. D. O'Connell, H. Wang, J. M. Martinis, and A. N. Cleland, Generation of Fock states in a superconducting quantum circuit, Nature (London) **454**, 310 (2008).
[56] F. Nogueira, Bayesian optimization: Open source constrained global optimization tool for PYTHON, https://github.com/fmfn/BayesianOptimization (2014).
[57] M. Hofheinz, H. Wang, M. Ansmann, R. C. Bialczak, E. Lucero, M. Neeley, A. D. O'Connell, D. Sank, J. Wenner, J. M. Martinis, and A. N. Cleland, Synthesizing arbitrary quantum states in a superconducting resonator, Nature (London) **459**, 546 (2009).
[58] M. Grant and S. Boyd, CVX: Matlab software for disciplined convex programming, version 2.1, http://cvxr.com/cvx (2014).
[59] I. Strandberg, Simple, reliable, and noise-resilient continuous-variable quantum state tomography with convex optimization, Phys. Rev. Appl. **18**, 044041 (2022).
[60] H. Wang, M. Mariantoni, R. C. Bialczak, M. Lenander, E. Lucero, M. Neeley, A. D. O'Connell, D. Sank, M. Weides, J. Wenner, T. Yamamoto, Y. Yin, J. Zhao, J. M. Martinis, and A. N. Cleland, Deterministic entanglement of photons in two superconducting microwave resonators, Phys. Rev. Lett. **106**, 060401 (2011).
[61] R. Lescanne, M. Villiers, T. Peronnin, A. Sarlette, M. Delbecq, B. Huard, T. Kontos, M. Mirrahimi, and Z. Leghtas, Exponential suppression of bit-flips in a qubit encoded in an oscillator, Nat. Phys. **16**, 509 (2020).
[62] P. Campagne-Ibarcq, A. Eickbusch, S. Touzard, E. Zalys-Geller, N. E. Frattini, V. V. Sivak, P. Reinhold, S. Puri, S. Shankar, R. J. Schoelkopf, L. Frunzio, M. Mirrahimi, and M. H. Devoret, Quantum error correction of a qubit encoded in grid states of an oscillator, Nature (London) **584**, 368 (2020).
[63] C. T. Hann, C.-L. Zou, Y. Zhang, Y. Chu, R. J. Schoelkopf, S. M. Girvin, and L. Jiang, Hardware-efficient quantum random access memory with hybrid quantum acoustic systems, Phys. Rev. Lett. **123**, 250501 (2019).
[64] V. V. Sivak, A. Eickbusch, H. Liu, B. Royer, I. Tsioutsios, and M. H. Devoret, Model-free quantum control with reinforcement learning, Phys. Rev. X **12**, 011059 (2022).
[65] X. Wu *et al.* (to be published).